Modification of the carrier mobility of conducting PF-EP polymer by formation of their composites with thiophene derivatives

Sergey Tokarev, Yury Fedorov, Anna Moiseeva, Gedaminas Jonusauskas, Dmitry Lypenko, Alexey Aleksandrov, Alexey Tameev, Eugene Maltsev, Galina Nosova, Elena Zhukova, et al.

Modification of the carrier mobility of conducting PF-EP polymer by formation of their composites with thiophene derivatives

Sergey D. Tokarev [a,b], Yury V. Fedorov [b], Anna A. Moiseeva [a], Gediminas Jonusauskas [c], Dmitry A. Lypenko [d], Alexey E. Aleksandrov [d], Alexey R. Tameev [d], Eugene I. Maltsev [d], Galina I. Nosova [e], Elena V. Zhukova [e], Olga A. Fedorova [a,b,*]

[a] Department of Chemistry, M. V. Lomonosov Moscow State University, Leninskie Gory, 119992, Moscow, Russia
[b] A. N. Nesmeyanov Institute of Organoelement Compounds, Russian Academy of Sciences, 28 Vavilova str., 119991, Moscow, Russia
[c] Laboratoire Ondes et Matière d'Aquitaine, UMR CNRS 5798, CNRS, University of Bordeaux, 351 Cours de la Libération, 33405, Talence, France
[d] A.N. Frumkin Institute of Physical Chemistry and Electrochemistry, Russian Academy of Sciences, Leninsky Prosp. 31, bld.4, 119071, Moscow, Russia
[e] Institute of macromolecular compounds, Russian Academy of Sciences, Bolshoy pr. 31, 199004, Saint-Petersburg, Russia

A B S T R A C T

In the paper we present synthesis and characterization of new donor–acceptor thiophene derivatives (TDs) containing vinylbenzo[d]thiazole, vinylpyridine and 1H-imidazo[4,5-*f*][1,10]phenanthroline residues. Using CELIV method, electron and hole mobility have been studied in the polymer layers based on poly [9,9-bis(6-diethoxyl-phosphorylhexyl)fluorine] (PF-EP) doped with the TDs. Polymer light-emitting diodes (PLEDs) containing newly synthesized polyfluorene (PF) as emitting layers and PF-EP/TD composites as electron transporting layers show higher brightness at 15V as compared with TD free PF-EP.

1. Introduction

Semiconducting polymers have several advantages such as mechanical flexibility, easy processing and transparency which help in the fabrication of cheaper flexible electronic devices [1]. The polymers has been recently applied for the production of various cheap OLEDs [2], transistors, energy storage elements [3], solar cells [4], chemical/biosensors [5], thermoelectric [6] and rechargeable batteries [7]. However, typical charge carrier mobility in these materials is low. Therefore, increased attention was directed to study hybrid assemblies based on semiconducting polymers with compounds like non-conducting macromolecules, metals, metal oxides/chalcogenides, carbonaceous and some other inorganic materials [8–12]. However, the success of these attempts has remained limited. Information on the advantageous use of small molecules as effective dopants in semiconducting polymer composites is still scarce.

Donor–acceptor (D-A) π-conjugated organic molecules are widely investigated as active materials in organic solar cells [13–20] for they are able to reduce the band gap [13,14,21]. Moreover, they were shown to be able to reach higher power conversion efficiency (PCE) and ease of device fabrication [22]. Another possible field of application is their use as active charge transport layers in organic flexible electronics [23,24]. Structure-properties correlations have been established for organic p-type, n-type and ambipolar molecules. In particular, organic semiconductors that exhibit both electron and hole transport are key components for the manufacture of complementary metal-oxide semiconductor (CMOS), digital integrated circuits [25–28] and organic light-emitting transistor (OLETs) devices [29–31].

Thiophene and its derivatives possess important electroluminescent characteristics. They are used as energy transfer and light-harvesting systems in various optical and electronic devices [32], as well as sensors and fluorescent markers [33–36]. Oligomeric thiophenes usually have good solubility and can be easily modified to fit various applications. For example, electron-donating (ED) and electron-withdrawing (EW) groups are used to tune the band gap and electron mobility of the oligomers. The intermolecular interactions and thin film morphology of these compounds change dramatically when ED or EW substituents are introduced [37]. Moreover, their position in oligomers is able to make different effects on the electronic properties [38].

Here, we synthesized and studied a series of mono- (**1a-d**) and bithiophene-containing derivatives (**2a-d**) (Scheme 1) constructed as donor–acceptor π-conjugated (D–π–A) systems for doping polymer

* Corresponding author. A. N. Nesmeyanov Institute of Organoelement Compounds, Russian Academy of Sciences, 28 Vavilova str., 119991, Moscow, Russia
E-mail address: fedorova@ineos.ac.ru (O.A. Fedorova).

matrix based on PF-EP. The synthesis of the polymer was given in Ref. [39]. Also the aim was to analyze the correlation between their structure, photophysical, electrochemical and charge transport properties in PE-EP composites. Earlier, the 2- or 3-styrylthiophene derivatives were used as initial reagents for obtaining polymers [40] and new near infrared compounds in bioimaging [41]. They were successfully applied in the analysis of TD excitation states [26,42] as well as efficient EL components [43].

2. Experimental

2.1. General

All reagents and solvents were purchased from Acros, Aldrich, Merck and used without additional purification. Spectroscopic grade acetonitrile (MeCN), DMSO, ethyl acetate were used for spectroscopic and fluorimetric measurements.

^{1}H and ^{13}C (APT method) NMR spectra were recorded on a Bruker AVANCE-400 and Avance-500 spectrometers. The chemical shifts and spin-spin coupling constants were determined with accuracy of 0.01 ppm and 0.1 Hz, respectively.

ESI mass spectra (ESI-MS) of **1a-d** and **2a,b** were acquired on a Finnigan LCQ Advantage tandem dynamic mass spectrometer (USA) equipped with a mass analyzer with an octapole ionic trap, a MS Surveyor pump, a Surveyor autosampler, a Schmidlin-Lab nitrogen generator (Germany), and a system of data collection and processing using the X Calibur program, version 1.3 (Finnigan). The mass spectra were measured in the positive ion mode. Samples in MeCN were injected directly into the source at flow rate 50 $\mu L \cdot min^{-1}$ through a Reodyne injector with a loop of 20 μL. The temperature of the transfer capillary was 150 °C, and the electrospray needle was held at potential 4.0 kV.

The electron impact mass spectra of **1a-d, 2a,b** were recorded on a Finnigan Polaris Q instrument. The energy of ionizing electrons was 70 eV. 1% solutions of compounds in CH_2Cl_2 or $CHCl_3$ (0.2 μl) were loaded into quartz micro-ampoules, which were inserted into the heated tip of the direct input rod. Thermomass spectrograms were filmed in the process of stepped (after 50°C) heating of ampoules from 50 to 150°C. Before heating the samples in the same temperature range, the thermomass spectrogram of the empty ampoule was usually taken to confirm an absence of any impurities in the ampoule and rod.

LDI-TOF mass spectra of **2c** and **2d** were collected with Bruker Autoflex II instrument, samples were irradiated with nitrogen laser (l = 337 nm). Isotopic patterns were calculated with Isotope Viewer 2000.

Elemental analysis was performed on a Carlo Erba 1108 elemental analyzer.

The synthesis of the copolymer PF (Scheme 2) was carried out in a Discover LabMate single-mode microwave reactor (CEM Corporation, United States) at a radiation frequency of 2.45 GHz and a maximum generator power of 300 W. The temperature of synthesis was controlled using an infrared sensor placed under the reaction vessel. The reaction parameters (temperature, power, time, stirring rate) were set manually. The molecular-mass characteristics of the copolymer were determined using size-exclusion liquid chromatography at 40°C on an Agilent Technologies 1260 Infinity chromatograph equipped with a refractometric detector. THF served as a mobile phase, molecular-mass characteristics were calculated using PS standards.

2.2. Synthesis

[2,2′-Bithiophene]-5,5′-dicarbaldehyde [44], 2,2′-bithiophene-5--carbaldehyde [44], 2,3-dimethylbenzo[d]thiazol-3-ium perchlorate [45], 7-methylbenzo[1,2-d:3,4-d']bis(thiazole)-2-amine [46] and 5, 5′-bis(1H-imidazo[4,5-f][1,10]phenanthrolin-2-yl)-2,2′-bithiophene (**2c**) [47] were prepared by using known synthetic procedures.

2.2.1. Synthesis of (E)-2-(2-([2,2′-bithiophen]-5-yl)vinyl)benzo[d] thiazole (1a)

Solution of 2,2′-bithiophen-5-carbaldehyde (1.55 mmol, 300 mg) and 2-methylbenzo[d]thiazole (1.55 mmol, 196 μl) in 7 ml of DMSO was stirred for 10 min, then 18.75 ml of 50% KOH water solution was added and the mixture was left without stirring for 2 days in the dark. After complete reaction the precipitate was filtered off, washed with water

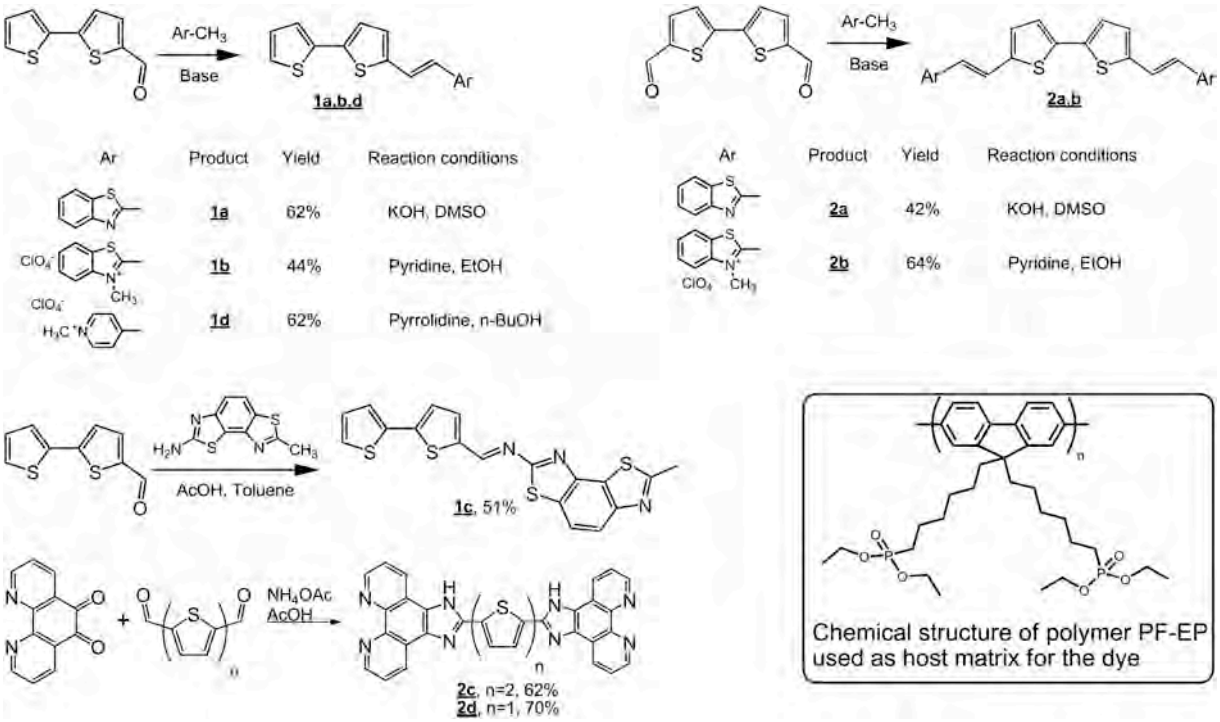

Scheme 1. Synthesis of dyes **1a-d**, **2a-d**, and structure of polymer host matrix.

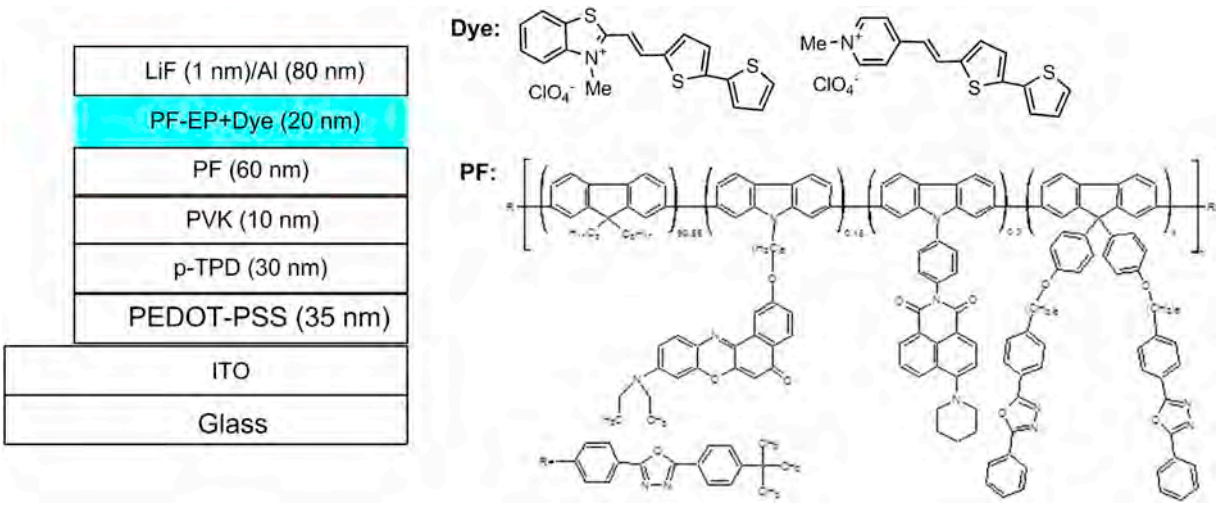

Scheme 2. Switch structure of OLED based on PF-EP + Dye composition.

and methanol and dried on a filter. The orange powder on a filter was a pure product (0.91 mmol, 297 mg, yield 62%). ^{1}H NMR ($CDCl_3$; δ; ppm, J/Hz): 7.04 (dd, 1H, $^3J = 3.8$, $^3J = 4.9$) H(4); 7.12–7.18 (m, 3H) H(a,b), H(3,3′,4′); 7.25 (d, 1H, $^3J = 3.4$) H(3,3′,4′); 7.27 (d, 1H, $^3J = 4.9$) H(5); 7.37 (dd, 1H, $^3J = 7.8$, $^3J = 7.6$), 7.48 (dd, 1H, $^3J = 7.6$, $^3J = 7.8$) H (6″,7″); 7.61–7.65 (d, 1h, $^3J = 15.9$) H(a,b); 7.85 (d, 1H, $^3J = 7.8$), 8.00 (d, 1H, $^3J = 7.8$) H(5″,8″).^{13}C NMR ($CDCl_3$; δ; ppm): 120.62; 121.47; 122.76; 124.39; 124.53; 125.26; 125.33; 126.40; 128.04; 130.06; 130.44 (CH); 119.28; 134.20; 136.85; 139.34; 141.96; 166.35 (C). Calculated for $C_{17}H_{11}NS_3$ (%): C, 62.73; H, 3.41; N, 4.30; found (%): C, 62.51 H, 3.67; N, 4.09. MS, *m/z* (%): calcd. 325.5; found 324.592 [M-H$^+$]$^-$ (100).

2.2.2. Synthesis of (E)-2-(2-([2,2′-bithiophen]-5-yl)vinyl)-3-methylbenzo [d]thiazol-3-ium perchlorate (1b)

Solution of 2,2′-bithiophene-5-carbaldehyde (0.77 mmol, 150 mg), 2,3-dimethylbenzo[d]thiazol-3-ium perchlorate (0.77 mmol, 203 mg) and 750 μl of pyridine in 7 ml of ethanol was refluxed for 30 h in darkness. Reaction mixture was evaporated dry on a rotary evaporator and 10 ml of methanol was added. Mixture was refluxed for 1 min to dissolve starting reagents and impurities. After filtering on a glass porous filter the pure product was obtained as a dark-brown precipitate (0.34 mmol, 149 mg, yield 44%). ^{1}H NMR (CD_3CN; δ; ppm, J/Hz): 4.18 (s, 3H) CH_3; 7.15 (dd, 1H, $^3J = 5.0$, $^3J = 3.7$) H(4); 7.29–7.33 (d, 1H, $^3J = 15.5$) H(a,b); 7.40 (d, 1H, $^3J = 4.0$), 7.48 (d, 1H, $^3J = 3.7$), 7.67 (d, 1H, $^3J = 4.0$) H(3,3′,4′); 7.52 (d, 1H, $^3J = 5.1$) H(5); 7.72–7.76 (dd, 1H, $^3J = 7.9$, $^3J = 8.4$), 7.82–7.86 (dd, 1H, $^3J = 8.5$, $^3J = 8.4$) H(6″, 7″); 7.97 (d, 1H, $^3J = 8.5$) H (5″,8″); 8.16–8.22 (m, 2H) H (5″,8″), H(a,b). ^{13}C NMR (CD_3CN; δ; ppm): 35.62 (CH_3); 109.83; 115.84; 123.31; 125.28; 126.07; 127.47; 128.19; 128.46; 129.26; 136.94; 140.83 (CH); 127.33; 135.34; 137.21; 141.77; 144.93 170.97(C). Calculated for $C_{18}H_{14}ClNO_4S_3$ (%): C, 49.14; H, 3.21; N, 3.18; found (%): C, 48.93 H, 3.42; N, 3.01. ESI-MS in MeCN, *m/z*: calcd. 340.03; found 340.071 [M]$^+$ (100).

2.2.3. Synthesis of (E)-N-([2,2′-bithiophen]-5-ylmethylene)-2-methylbenzo[1,2-d:3,4-d']bis(thiazole)-7-amine (1c)

7-Methylbenzo[1,2-d:3,4-d']bis(thiazole)-2-amine (0.9 mmol, 200 mg) and 2,2′-bithiophene-5-carbaldehyde (0.9 mmol, 176 mg) were separately dissolved in toluene, in case of the amine a little heating was required. Toluene solutions were mixed and 3 ml of glacial acetic acid was added. Reaction solution was refluxed for 30 h, after complete reaction solvent was removed on a rotary evaporator, 10 ml of ethanol were added and mixture was refluxed for 5–10 min. The precipitate formed was filtered on a glass porous filter and washed with ethanol. The pure product was obtained by flash chromatography (SiO_2, benzene: acetonitrile = 12:1), 0.459 mmol, 182 mg, yield 51%. ^{1}H NMR (DMSO-d_6; δ; ppm, J/Hz): 2.88 (s, 3H) CH_3; 7.19 (dd, 1H, $^3J = 5.0$, $^3J = 3.7$) H(4); 7.55 (d, 1H, $^3J = 3.97$), 7.61 (d, 1H, $^3J = 3.6$), 7.99 (d, 1H, $^3J = 3.9$) H(3,3′,4′); 7.71 (d, 1H, $^3J = 5.1$) H(5); 7.93 (d, 1H, $^3J = 8.7$), 8.15 (d, 1H, $^3J = 8.6$) H(7″,8″). ^{13}C NMR (DMSO-d_6; δ; ppm): 19.83 (CH_3); 119.24; 120.23; 125.54; 126.84; 128.30; 128.95; 139.68; 159.14 (CH); 126.34; 131.54; 135.55; 138.83; 144.85; 146.07; 150.54; 169.93; 170.37 (C). Calculated for $C_{18}H_{11}N_3S_4$ (%): C, 54.38; H, 2.79; N, 10.57; found (%): C, 54.18 H, 2.93; N, 10.30. MS, *m/z* (%): calcd. 397.5; found 396.516 [M-H$^+$]$^-$ (100).

2.2.4. Synthesis of (E)-4-(2-([2,2′-bithiophen]-5-yl)vinyl)-1-methylpyridin-1-ium perchlorate (1d)

Mixture of 2,2′-bithiophen-5-carbaldehyde (1.97 mmol, 383 mg), 1,4-dimethylpyridin-1-ium perchlorate (1.97 mmol, 410 mg), pyrrolidine (1.97 mmol, 140 μl) in 10 ml of n-butanol was refluxed for 30 min in darkness. The precipitate formed was filtered on a glass porous filter, washed with methanol, dried on a filter and recrystallized from acetonitrile/benzene mixture. The pure product was obtained as an orange powder (1.22 mmol, 468 mg, yield 62%). ^{1}H NMR (CD_3CN; δ; ppm, J/Hz): 4.16 (s, 3H) CH_3; 6.99–7.03 (d, 1H, $^3J = 16.0$) H(a,b); 7.11 (dd, 1H, $^3J = 3.7$, $^3J = 5.1$) H(4); 7.28 (d, 1H, $^3J = 3.9$), 7.37–7.39 (m, 2H) H (3,3′,4′); 7.44 (d, 1H, $^3J = 5.3$) H(5); 7.88–7.92 (m, 3H) H(a,b), H (2″,3″,5″,6″); 8.37 (d, 2H, $^3J = 7.0$) H(2″,3″,5″,6″). ^{13}C NMR (CD_3CN; δ; ppm): 48.07 (CH_3); 122.17; 124.27; 126.03; 126.38; 127.61; 129.28; 134.48; 134.71; 145.46 (CH); 129.55; 137.12; 140.09; 142.07 (C). Calculated for $C_{16}H_{14}ClNO_4S_2$ (%): C, 50.06; H, 3.68; N, 3.65; found (%): C, 49.90 H, 3.86; N, 3.38. ESI-MS in MeCN, *m/z*: calcd. 284.42; found 283.922 [M]$^+$.

2.2.5. Synthesis of 5,5′-bis((E)-2-(benzo[d]thiazol-2-yl)vinyl)-2,2′-bithiophene (2a)

[2,2′-Bithiophene]-5,5′-dicarbaldehyde (0.45 mmol, 100 mg) and 2-methylbenzothiazol (0.9 mmol, 134 mg) were dissolved in DMSO, stirred for 10 min and an aqueous 50% solution of KOH (4 ml) was added. Two-layered mixture stayed with no stirring for 2 days. After complete reaction, the precipitate formed was filtered on a glass porous filter, washed with water and methanol. After washing the sediment was transferred into the flask, 1 ml of benzene, carbon tetrachloride, ethyl acetate and methanol each was added to it. The mixture was subjected to ultrasonic treatment for 10 min at 40°C in darkness, filtered and dried on a rotary evaporator. The pure product was obtained as a red-brown precipitate (0.19 mmol, 92 mg). Yield 42%. ^{1}H NMR (DMSO; δ; ppm, J/Hz): 7.28 (d, 2H, $^3J = 15.7$) H(a,b); 7.44 (t, 2H, $^3J = 7.8$, $^3J = 7.5$) H (5,6); 7.46 (d, 2H, $^3J = 3.7$) H (1′,2′); 7.51–7.54 (m, 4H) H(1′,2′,5,6);

7.84 (d, 2H, $^3J = 15.9$) H(a,b); 7.96 (d, 2H, $^3J = 8.3$), 8.07 (d, 2H, $^3J = 7.8$) H(4,7). Due to the low solubility of the product, it was not possible to characterize it by means of ^{13}C NMR spectroscopy. Calculated for $C_{26}H_{16}N_2S_4$ (%): C, 64.43; H, 3.33; N, 5.78; found (%): C, 64.20 H, 3.51; N, 5.54. MS in MeCN, *m/z*: calcd. 484.6; found 483 608 $[M\text{-}H^+]^-$.

2.2.6. Synthesis of 2,2'-((1E,1′E)-[2,2′-bithiophene]-5,5′-diylbis(ethene-2,1-diyl))bis(3-methylbenzo[d]thiazol-3-ium) (2b)

Mixture of [2,2′-bithiophene]-5,5′-dicarbaldehyde (0.315 mmol, 70 mg), 2,3-dimethylbenzo[d]thiazol-3-ium perchlorate (0.63 mmol, 166.2 mg) and 700 μl of pyridine in 5 ml of ethanol was refluxed for 12 h in darkness. After the removing of solvent on a rotary evaporator, the sequence of boiling in 5 ml of ethanol for 5 min and filtering was repeated twice. The pure product was obtained as a black-violet precipitate (0.2 mmol, 143 mg), yield 64%. ^1H NMR (DMSO; δ; ppm, J/Hz): 4.33 (s, 6H) CH_3; 7.75–7.82 (m, 6H) H(4,5,6,7,a,b); 7.89 (dd, 2H, $^3J = 7.8$, $^3J = 7.4$) H(5,6); 8.02 (d, 2H, $^3J = 3.9$) H(1′,2′); 8.24 (d, 2H, $^3J = 8.0$) H(4,7); 8.42–8.49 (m, 4H) H(1′,2′,a,b). ^{13}C NMR (DMSO δ; ppm): 36.29 (CH_3); 116.79; 124.26; 127.87; 128.42; 136.56; 139.80; 142.05; 170.85 (CH); 112.78; 128.05; 129.46; 139.91; 142.17 (C). Calculated for $C_{28}H_{22}Cl_2N_2O_8S_4$ (%): C, 47.12; H, 3.11; N, 3.93; found (%): C, 46.96 H, 3.24; N, 3.72. ESI-MS in MeCN, *m/z*: calcd. 514.7; found 257.295 $[M]^{2+}$.

2.2.7. Synthesis of 2,5-bis(1H-imidazo[4,5-f][1,10]phenanthrolin-2-yl) thiophene (2d)

1,10-phenanthroline-5,6-dione (3 mmol, 0.6 g) was added to the hot solution of thiophene-2,5-dicarbaldehyde (1.5 mmol, 210 mg) and ammonia acetate (30 mmol, 2.31 g) in 20 ml of glacial acetic acid. The mixture was refluxed for 6 h and cooled to the room temperature. Water solution of ammonia (15%) was added to pH∼8. The precipitate formed was filtered on a glass porous filter, washed with water and methanol. The remaining sediment was refluxed in 40 ml of methanol for 30 min. By filtering hot mixture on a glass porous filter the pure product was obtained as a grey-brown powder (1.05 mmol, 548 mg, yield 70%) ^1H NMR (DMSO-d_6; δ; ppm, J/Hz): 7.85–7.88 (dd, 4H, $^3J = 4.2$, $^3J = 8.1$) H (5′,5″,10′,10″); 8.01 (s, 2H) H(3,4); 8.88 (d, 4H, $^3J = 8.0$) H (4′,4″,11′,11″); 9.05 (d, 4H, $^3J = 4.0$) H(6′,6″,9',9"). Due to the low solubility of the product, it was not possible to characterize it by means of ^{13}C NMR spectroscopy. Calculated for $C_{30}H_{16}N_8S$ (%): C, 69.22; H, 3.10; N, 21.53; found (%): C, 69.14 H, 3.21; N, 21.31. MALDI-MS *m/z*: 522 $[M+H]^+$, 544 $[M+Na]^+$.

2.3. Absorption and emission spectra

UV–Vis spectra were measured using a two channel spectrophotometer Varian-Cary 300 and an Avantes AvaSpec-2048 spectrophotometer. Fluorescence spectra were measured at 20 ± 1°C with a FluroLog-3-221(Horiba Scientific) and Agilent Cary Eclipse spectrofluorometers.

2.4. Determination of quantum yield of the $E \rightleftarrows Z$ photoisomerization

To determine the quantum yields of the forward and backward reactions of $E \rightleftarrows Z$ photoisomerization of **1a** and **1d**, we preliminarily calculated the absorption spectra of the corresponding *Z*-isomer and the ratios of quantum yields for the forward and backward reactions of $E \rightleftarrows Z$-photoisomerization using the Fisher method [48] from the absorption spectra of the *E*-isomer and the spectra of two photostationary states obtained by photoirradiation at two different wavelengths.

2.5. Fluorescence quantum yield

All measured fluorescence spectra were corrected for nonuniformity of detector spectral sensitivity. Anthracene ($\phi_{fl} = 0.27$), tris(bipyridine) ruthenium(II) chloride ($\phi_{fl} = 0.028$), coumarine 6 ($\phi_{fl} = 0.78$) and rhodamine 6G ($\phi_{fl} = 0.95$) in ethanol were used as references for the fluorescence quantum yield measurements.

2.6. Fluorescence decay measurements

Fluorescence decay measurements of **1a-d** in MeCN were carried out using the following system. A Ti:sapphire laser system emitting pulses of 0.6 mJ and 30 fs at 800 nm and 1 kHz pulse repetition rate (Femtopower Compact Pro) with home-built optical parametric generator and frequency mixers was used to excite the samples at the maximum of the steady-state absorption band. All excited-state lifetimes were obtained by using depolarized excitation light. The highest pulse energies used to excite fluorescence did not exceed 100 nJ and the average power of excitation beam was 0.1 mW at a pulse repetition rate of 1 kHz focused into a spot with a diameter of 0.1 mm in the 10 mm-long fused-silica cell. The fluorescence emitted in the forward direction was collected by reflective optics and focused with a spherical mirror onto the input slit of a spectrograph (Chromex 250) coupled to a streak camera (Hamamatsu 5680 equipped with a fast single sweep unit M5676, temporal resolution 2 ps). Convolution of a rectangular streak camera slit in the sweep range of 250 ps with electronic jitter of the streak camera trigger pulse provided a Gaussian (over four decades) temporal apparatus function with a full width at half-maximum of 20 ps. The fluorescence kinetics were later fitted by means of the Levenberg–Marquardt least-squares curve-fitting method using a solution of the differential equation describing the evolution in time of a single excited state and neglecting depopulation of the ground state according to Eq. (1),

$$\frac{dI}{dt} = Gauss(t_0, \Delta t, A) - \frac{I(t)}{\tau} \quad (1)$$

where $I(t)$ is the fluorescence intensity, *Gauss* is the Gaussian profile of the excitation pulse, in which t_0 is the excitation pulse arrival delay, Δt – the excitation pulse width, and A – the amplitude. The parameter τ is the lifetime of the excited state. The initial condition for the equation is $I(-\infty) = 0$. Typically, the fit shows a χ^2 value (Pirson's criteria) better than 10^{-4} and a correlation coefficient $R > 0.999$. The uncertainty of the lifetime was better than 1%. Routinely, the fluorescence accumulation time in our measurements did not exceed 90 s.

Fluorescence decay measurements of **2a-d** in MeCN were carried out using a spectrofluorometer FluoroLog-3-221 (Horiba Scientific) equipped with Time-Correlated Single Photon Counting (TCSPC) module and solid-state pulsed NanoLED emitting at 455 nm and 1 MHz pulse repetition rate. To determine fluorescence lifetimes the fluorescence kinetics were analyzed by fitting the decay curves with the use of the DAS6 program. The relative accuracy of the lifetime measurements done under the same conditions was ±0.01 ns.

2.7. Voltammetry studies

Electrochemical measurements were carried out at 22 C with an IPC-ProM potentiostat. Cyclic voltammetry experiments were performed in a 1.0 mL cell equipped with a glassy carbon (GC) electrode (disk d = 2 mm), Ag/AgCl/KCl (aq. saturated; reference electrode), and platinum electrode (counter electrode). Compounds were dissolved in degassed dry CH_3CN or DMF containing TBAP as the supporting electrolyte (0.1 M). Dry argon gas was bubbled through the solutions for 30 min before cyclic voltammetry experiments. The scan rate was 200 mV s^{-1}.

2.8. Charge carrier mobility and conductivity measurements

In thin layers of the composites, charge carrier mobility (μ) was measured by using the technique of charge extraction by linearly

increasing voltage (CELIV) with metal-insulator-semiconductor (MIS) diode structures. A thin layer ($d_s = 130$ nm) of the PF-EP/TD composite (5 wt %) was deposited onto the SiO_2/ITO/glass substrate by spin coating of the 5 mg/ml solution in the ethanol/acetonitrile (95/5 vol) mixture at rate of 1000 rpm and dried at 60 °C for 3h. Then a 80 nm thick Al top electrode was deposited onto the composite layer by thermal evaporation under 10^{-6} mbar vacuum at rate of 1 Å/s. A charge carrier blocking SiO_2 layer of 70 nm thick was preliminary deposited onto ITO-coated glass by magnetron scattering at 10^{-3} mbar.

The CELIV set-up included a digital USB-oscilloscope (DL-Analog Discovery, Digilent Co.), which played roles of master pulse generator and transient current pulse monitor. *RC* constants were at least a factor of 20 smaller than the time scales of interest. The bias was swept in the range between 10 and 100 kHz.

A small charge extraction regime of the MIS-CELIV experiment was used. The condition $\Delta j \leq j(0)$ where Δj is a maximum current of unipolar charge carriers and $j(0)$ is a capacitance current [49]. The corresponding small-charge transit time t_{max} for the sheet of carriers to reach the extracting contact defines the mobility as following [49]:

$$\mu = \frac{2d_s^2}{(At_{max}^2)(1+f)}$$

where the ratio between the geometric capacitances of the organic semiconductor and the SiO_2 insulator layers $f \equiv (\varepsilon_s\ d_i)/(\varepsilon_i\ d_s)$ is ranged between ~ 0.34 and ~0.45 for dielectric constants ε_i is $\varepsilon_i =$ 3.9 and $\varepsilon_s =$ ~2.5 for SiO_2 and PF-EP/TD (5 wt%) composite, respectively.

The electrical conductivity of thin films was measured using the four-probe technique in the 4-stripe layout as described in Ref. [50]. The Al electrodes were made as parallel stripes of 10 mm in width with equal distance of 0.7 mm between neighbors. The outer and inner pairs of the electrodes served as current and voltage contacts, respectively. Electrical measurements were carried out in a glovebox with Ar atmosphere at room temperature using Keithley 236 and 2400 source-meter units and a standard probe station (MPI ITS50COAX) setup. The thickness of the films was ranged between 100 and 120 nm. The relative error of the conductivity measurements was 15%.

2.9. OLED devices fabrication and characterization

PEDOT:PSS solution (Heraeus, Clevios P VP. Al 4083) was spin-coated onto the ITO-coated glass substrates at 2000 r.p.m. for 60 s and baked at 110 °C for 30 min. The PEDOT:PSS-coated substrates were transferred into an argon-filled glove box ($O_2 <$ 1p.p.m., $H_2O <$ 1 p.p.m.). Poly-TPD in chlorobenzene (8 mg/ml) and PVK in o-xylene (1.5 mg/ml) were deposited layer by layer by spin coating at 2000 r.p.m. for 45 s. Deposited in succession poly-TPD and PVK layers were baked at 110 °C for 20 min and at 140 °C for 30 min, respectively. A PF layer was spin-cast over PVK layer from a toluene solution at 1500 r.p.m for 1 min and dried at 80 °C for 3 h. Then a 20 nm thick layer of the PF-EP/TD composite (5 wt%) was deposited by spin coating of 5 mg/ml solution in the ethanol/acetonitrile (95/5% vol.) mixture at rate of 1000 r.p.m and dried at 60 °C for 3h. Finally LiF (1 nm)/Al(80 nm) cathode was deposited onto the composite layer through a shadow mask by thermal evaporation under 2×10^{-6} mbar vacuum. The device area was 9 mm^2.

The EL spectra of OLEDs were recorded on an Avantes 2048 fiber-optic spectrofluorimeter (Netherlands). Voltage–current and voltage–-brightness characteristics were measured with Keithley 2601 Source-Meter (USA), Keithley 485 pico-ammeter and TKA-04/3 luxmeter-brightness meter (Russia). The thicknesses of the films were determined using MII-4 interferometer (LOMO, St.-Petersburg, Russia). The preparation of OLED samples and measurements of their spectral and opto-electronic characteristics were performed at room temperature under argon atmosphere.

3. Results and discussion

Mono- (**1a-d**) and bisubstituted thiophene containing TDs **2a-d** were synthesized as shown on Scheme 1. Synthesis includes the condensation reaction of 2,2′-bithiophene-5-carbaldehyde or 2,2′-bithiophene-5,5′-dicarbaldehyde with 2-methylbenzo[d]thiazole, 7-methylbenzo[1,2-d:3,4-d']bis(thiazole)-2-amine, 2,3-dimethylbenzo[d]thiazol-3-ium perchlorate, 1,4-dimethylpyridin-1-ium perchlorate and 1,10-phenanthroline-5,6-dione (see Experimental part). TD **2d** is the only containing one thiophene moiety. TD **2c** is known in literature [47]. The other TDs were synthesized for the first time. Their structures were proved by ^1H, ^{13}C NMR, ESI-MS, elemental analysis.

3.1. Optical and electrochemical properties

The absorption and emission maxima of TDs **1a-d** and **2a-d** are listed in Table 1 and Figs. S1–S16 in ESI. Comparing the absorption data for TDs **1a** and **1c**, it can be seen that the replacement of the benzothiazole ring by a benzobis(thiazole) leads to a bathochromic shift up to 33 nm, related to an increased size of heterocyclic residue in compound **1c**. Also, TD **2a** possessing two vinylbenzothiazole residues demonstrates the long wavelength absorption band which is 65 nm bathochromically shifted compared to **1a**. The long wavelength absorption band for positive charged TDs **1b,d** and **2b** was shifted bathochromically relative to neutral TDs **1a**, **2a**. In case of TDs **2c** and **2d** the bathochromic shift of long wavelength absorption band is observed when going from **2d** to **2c** as the number of thiophene units increased, as expected from the increase of conjugation length. The same trend was observed in the emission spectra of these compounds as the position of the wavelength of maximum emission was red-shifted for each added thiophene,

Table 1
Optical and electrochemical characteristics of TDs **1a-d** and **2a-d**. E_{pc} and E_{pa} stand for redox potentials of compounds, $\lambda^{abs}{}_{max}$ and $\lambda^{fl}{}_{max}$ – absorption and fluorescence peaks maxima respectively, Φ_{fl} and $\Phi_{E\text{-}Z}/\Phi_{Z\text{-}E}$ – quantum yields of fluorescence and *E-Z/Z-E* isomerization respectively, T – fluorescence lifetimes.

TD	E_{red}, V[a]	E_{ox}, V	$\lambda^{abs}{}_{max}$, nm[b]	$\lambda^{fl}{}_{max}$, nm	Φ_{fl}, %	$\Phi_{E\text{-}Z}/\Phi_{Z\text{-}E}$, %	T, ps
1a	−1.50 −1.80	1.14 1.49 1.69	386	498	0,2	55/13	30
1b	−0.58 −1.87	1.41 1.79	472	597	0,5	[c]	30
1c	−1.10 −1.49	1.88	419	485	11.5	–	7, 770 (12%)
1d	−0.87 −1.53	1.37 1.75	431	579	2,0	55/56	83, 163 (31%)
2a	−1.30/-1.21 −1.50 −1.83	1.20 1.41	451	550	10,3	[d]	570
2b	−0.41/-0.35 −1.72	1.69 1.77	525	619	8,4	[c]	320
2c	−1.12 −1.39	0.91 1.17 1.31	400, 423	640	23,3	-	1260 (8.3%) 2700 (91.7%)
2d	−0.88 −1.41	0.51 1.09 1.26	388	535	29,7	-	2100

[a] Electrochemical characteristics were measured in MeCN (**1a-c, 2b)** or DMF (**2a,c,d**).
[b] Optical spectra were recorded in MeCN.
[c] Fast back *cis-trans*-reaction.
[d] Photoisomerization process included isomerization around two double C=C bonds.

increase of the heterocyclic residue size and replacement of neutral residue with positively charged (Table 1). The synthesized compounds showed large Stokes' shift (the lowest being for **1c** and the highest for **2d**). A large Stokes shift is an important characteristic for a fluorescent probe that allows an improved separation of the light inherent to the matrix and the light dispersed by the sample [50].

The measured fluorescence quantum yields have values ranging from 0.2 to 29.7%. . Irradiation of TDs **1a,d** with light at 405 nm and 436 nm, respectively, causes *E,Z*-photoisomerization with a fairly high quantum yield (0.55), while reverse *Z,E*-photoisomerization is less effective for **1a** and comparable to direct photoisomerization for **1d** (Table 1 . Compounds **1b** and **2b** also demonstrate the *E,Z*-photoisomerization with high rate of the reverse isomerization in the dark .
In case of **2a** the photoisomerization occurs with participation of two double bonds [26,34,42],

Some experiments were carried out by ultrafast techniques (Table 1) in order to reveal the possible role of upper excited states and/or primary steps involving precursor transients. Only the $S_1 \rightarrow S_n$ transient was observed for **1a-c**, with a decay rate corresponding to the fluorescence lifetime. The other TDs possess longer lifetime of fluorescence. In case of **2c,d** temporal range can indicate a fast ISC and irradiative relaxation of exited state.

The redox properties of **1a-d, 2a,b** were investigated by cyclic wave voltammetry in MeCN or DMF containing tetrabutylammonium perchlorate as supporting electrolyte. The resulting electrochemical data are summarized in Table 1. The HOMO and LUMO energy levels are compiled in Table 2. From Table 2, the band gaps of **1a-d** and **2a-d** lay from 1.39 eV (**2d**) up to 2.98 eV (**1c**), which are in good agreement with the optical band gaps. In series of **1a-d** compounds, **1b** with stronger electron withdraw benzothiazolium heterocyclic group results in a lower LUMO level of −4.15 eV and a narrower band gap (1.99 eV). In case of compounds **2a-d**, lower LUMO level of −4.32 eV belongs to **2b**, whereas, a narrower band gap (1.39 eV) was observed for **2d**.

3.2. The charge transport study

PF-EP was used as a wide band-gap polymer matrix with HOMO and LUMO levels of −5.7 eV and −2.2 eV [51], respectively. That is why the studied materials exhibited low electrical conductivity. The 4-probe technique measurements showed that it equals to 6×10^{-5} S/cm for the PF-EP films and ranges between 7×10^{-5} and 1×10^{-4} S/cm for PF-EP/TD thin films . To determine charge carriers mobility we used the MIS-CELIV technique [52–54]. Due to the presence of electron donor and acceptor moieties in the molecules (Table 2), they exhibit ambipolar charge transporting properties. HOMO and LUMO levels afford the hopping transport of holes and electrons, respectively.

The electron mobility values in all the PF- EP/TD composites, except for PF- EP/**1d**, are larger than that in the PF-EP. We believe that the main reasons for the enhancement of the charge mobility are following: (a) TDs themselves serve as charge transport sites, (b) charge-transfer states formed by TDs and PF-EP are involved in the transport. According to the concentration of TDs in the polymer, the mean distance between neighboring molecules does not exceed 2 nm provided they are distributed uniformly. That is why they are really able to participate in the electron transport. Moreover, the LUMO levels of the TDs are located at least 1eV lower than that of PF-EP, so the polymer matrix does not hamper the electron transport. The hole mobility in the PF-EP/TD composites appeared to be lower than that for the PF-EP. Since the HOMO level of the PF-EP is located about 1eV higher than that of PF-EP/TD, the TDs serve as hole traps. Thus, basing on the conductivity and charge carrier mobility data, we reveal that a few tens nanometers thick layer of such materials can serve as an ETL.

Table 2
LUMO-HOMO levels (eV) for TDs and charge carrier mobility ($cm^2V^{-1}s^{-1}$) in PF-EP doped with TDs (5 wt %).

Material	LUMO	Electron mobility	HOMO	Hole mobility
PF-EP	−2.2 ÷ −3.0	$2.50 \cdot 10^{-5}$	−5.7	$1.94 \cdot 10^{-4}$
PF- EP+**1a**	−3.23	$1.50 \cdot 10^{-4}$	−5.87	$3.27 \cdot 10^{-5}$
PF- EP+**1b**	−4.15	$9.43 \cdot 10^{-5}$	−6.14	$1.42 \cdot 10^{-4}$
PF- EP+**1c**	−3.63	$2.34 \cdot 10^{-4}$	−6.61	$7.15 \cdot 10^{-5}$
PF- EP+**1d**	−3.86	$1.05 \cdot 10^{-5}$	−6.10	$6.45 \cdot 10^{-5}$
PF- EP+**2a**	−3.43	–	−5.93	$9.50 \cdot 10^{-6}$
PF- EP+**2b**	−4.32	–	−6.42	$4.30 \cdot 10^{-6}$
PF- EP+**2c**	−3.61	$6.00 \cdot 10^{-5}$	−5.64	$1.30 \cdot 10^{-5}$
PF- EP+**2d**	−3.85	$1.09 \cdot 10^{-4}$	−5.24	$3.28 \cdot 10^{-5}$

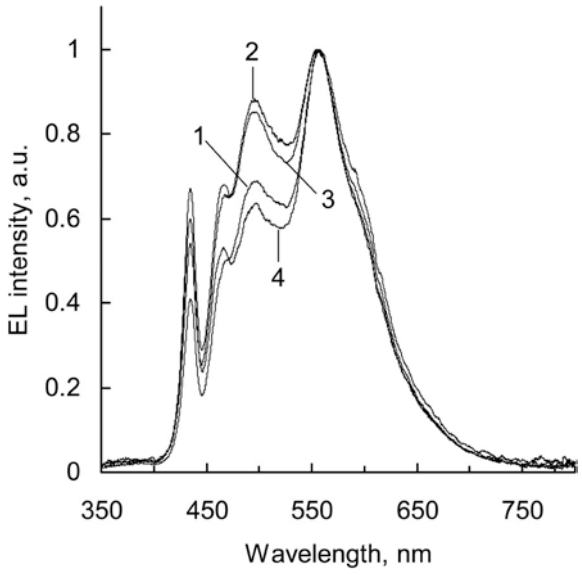

Fig. 1. EL spectra of the studied PLED that has no TD component in the PF-EP electron. transport layer (1) and three other samples with **1a** (2), **1b** (3) and **1d** (4).

Table 3
EL characteristics of the studied PLEDs with different electron injection/transport layers.

Electron transport layer	U_{on}, V	Brightness, cd/m^2 U = 15V	Max. efficiency		CIE, x, y	λ_{max} EL, nm
			Current cd/A	Luminousity lm/W		
PF-EP	10	1080	1.01	0.26	0.340 0.433	435, 465, 494, 556, 598
PF-EP +**1a**	13	970	0.17	0.03	0.313 0.416	435, 465, 494, 556, 598
PF-EP +**1b**	9	1770	0.64	0.17	0.311 0.403	435, 465, 494, 556, 598
PF-EP +**1d**	8.5	1910	0.54	0.17	0.341 0.411	435, 465, 494, 556, 598

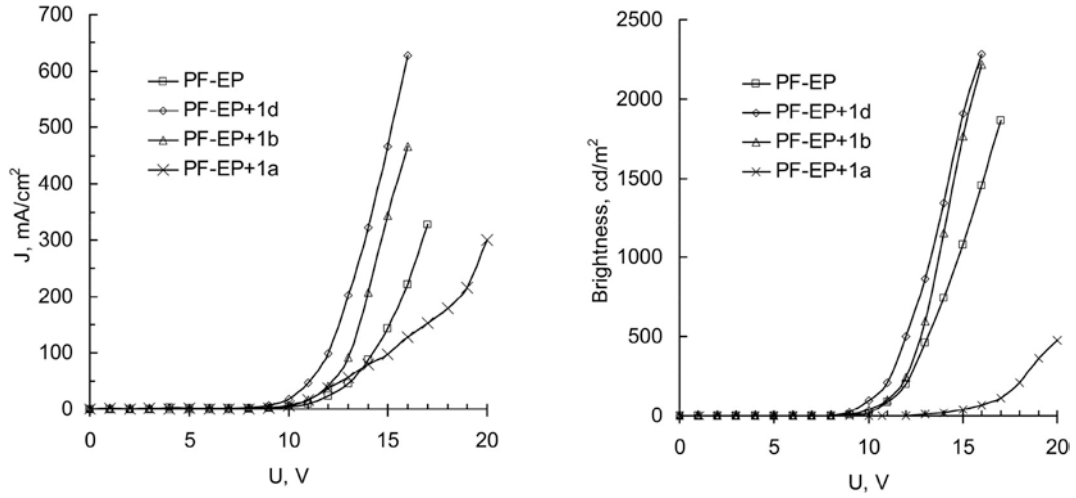

Fig. 2. Voltage-current and voltage-brightness characteristics of the PLED that has no dye component in the PF-EP electron transport layer and three other samples with **1a**, **1b** and **1d**.

3.3. Styrylthiophene in composition of polymer light-emitting diodes (PLEDs)

Conjugated polyelectrolytes and organic salts attract particular attention due to their use as efficient electron injection/transport layers [55,56]. We investigated the effect of styrylthiophen-containing derivatives in the electron injection/transport layers on the EL characteristics of PLEDs. A series of EL structures containing a polyfluorene derivative (PF) as a light-emitting layer (Scheme 2) was manufactured. Concentration of the TDs in the composites was 5% by weight. The PLEDs exhibited electroluminescence in the entire visible spectral region (Fig. 1).

Composites based on PF-EP and **1a**, 1**b and 1d** were used as electron transport layers (ETLs). The EL spectra of the PLEDs slightly differ (Fig. 1). Table 3 shows that for a series of samples with **1b** and **1d**, luminescence voltage onsets decrease and equal 9 and 8.5 V, respectively, in contrast to the ETL based on the pure PF-EP (10V) and composite containing **1a** (13V) (Fig. 2). It is noteworthy, that at the voltage of 15 V, brightness of the samples in the presence of **1b** and **1d** was twice as high as that of a PLED with pure PF-EP. For the most of PFs with different substituents, the HOMO and LUMO levels are in the range −5.5 to −5.7 eV, and −2.5 to −3 eV, correspondingly [57]. The LUMO levels of the compounds **1b** and **1d** of −4.15 and −3.86 eV, respectively, act as levels that promote electron injection into the composite from Al (work-function 4.3 eV). The TD **1a** with the LUMO level of −3.23 eV, on the other hand, does not improve the electron transfer to PF-EP. While the electron and hole mobility imbalance increases in the PF-EP+**1a** composite (Table 2), both the current density and brightness of the PF-EP+**1a** based PLED decrease compared with those of the PF-EP based PLED.

4. Conclusion

We have synthesized mono- and bisubstituted thiophene derivatives containing a π-electron donor thiophene moiety (or moieties) connected through a double bond as a linker with a π-electron heterocyclic acceptor and studied them as dopants in the conducting polymer layers of PF-EP.

The photophysical and electrochemical measurements allowed us to obtain new data on the optical properties of these compounds and determine their frontier-orbital energy levels. It was revealed that the prepared compounds are able to participate in *E,Z*-photoisomerization. The neutral derivatives **1a, 1c and 2a** possess larger fluorescence quantum yields as compare with positively charged molecules **1b**, 1**d** and **2b**. All they demonstrate a large Stocks shift.

We have found that incorporation of TD molecules into the PF-EP polymer improves electron transport in the composite. In particular, for composites with TDs **1a**, **1b**, **1c**, **1d**, the electron mobility increases in the following sequence **1d** < TD free <**1b** < **1a** <**1c** (Table 2). However, in the operating voltage mode on LEDs with ETLs containing these composites, the current and brightness increase in the sequence **1a** < TD free <**1b** < **1d** (Fig. 2). This indicates that it is the effective electron injection due to the lower lying LUMO levels of TDs (namely, **1b** and **1d**) relative to the LUMO level in the PF-EP and not electron transport in the ETLs plays a key role in the operation of the manufactured LEDs.

The light–emitting diodes made of PF-EP composites containing **1b** and **1d** showed almost two times higher brightness at 15V when compared with a diode made of pure PF-EP.

Thus, the vinylthiophene derivatives containing heterocyclic acceptor substituents let one to produce the compounds that improve ambipolar charge transport. The further synthesis and analysis of such structures may be considered as a promising approach to the development of new electroactive composites with better optoelectronic characteristics.

Declaration of competing interest

The authors declare that they have no known competing financial interests or personal relationships that could have appeared to influence the work reported in this paper.

Acknowledgments

Financial support from the Russian Science Foundation (RSF № 17-73-30036) and equipment facilities from Center of collective facilities of A. N. Nesmeyanov Institute of Organoelement compounds of Russian Ministry of Sciences and High Education are gratefully acknowledged.

References

[1] S.R. Forrest, The path to ubiquitous and low-cost organic electronic appliances on plastic, Nature 428 (2004) 911–918.

[2] J.H. Burroughes, D.D.C. Bradley, A.R. Brown, R.N. Marks, K. Mackay, R.H. Friend, et al., Light-emitting-diodes based on conjugated polymers, Nature 347 (1990) 539–541.

[3] Y.G. Li, W. Zhou, H.L. Wang, L.M. Xie, Y.Y. Liang, F. Wei, et al., An oxygen reduction electrocatalyst based on carbon nanotube-graphene complexes, Nat. Nanotechnol. 7 (2012) 394–400.

[4] M. Skompska, Hybrid conjugated polymer/semiconductor photovoltaic cells, Synth. Met. 160 (2010) 1–15.

[5] D.W. Hatchett, M. Josowicz, Composites of intrinsically conducting polymers as sensing nanomaterials, Chem. Rev. 108 (2008) 746–769.

[6] Z.U. Khan, J. Edberg, M.M. Hamedi, R. Gabrielsson, H. Granberg, L. Wagberg, Thermoelectric polymers and their elastic aerogels, Adv. Mater. 28 (2016) 4556–4562.

[7] G. Wang, L. Zhang, J. Zhang, A review of electrode materials for electrochemical supercapacitors, Chem. Soc. Rev. 41 (2012) 797–828.

[8] R. Gangopadhyay, A. De, Conducting polymer nanocomposites: a brief overview, Chem. Mater. 12 (2000) 608–622.

[9] C. Janaky, K. Rajeshwar, The role of (photo) electrochemistry in the rational design of hybrid conducting polymer/semiconductor assemblies: from fundamental concepts to practical applications, Prog. Polym. Sci. 43 (2015) 96–135.

[10] X. Ji, Y. Xu, W. Zhang, L. Cui, J. Liu, Review of functionalization, structure and properties of graphene/polymer composite fibers, Composites, Part A 87 (2016) 29–45.

[11] K. Rajeshwar, N.R. De Tacconi, C.R. Chenthamarakshan, Semiconductor-based composite materials: preparation, properties, and performance, Chem. Mater. 13 (2001) 2765–2782.

[12] P. Gomez-Romero, Hybrid organic–inorganic materials –in search of synergic activity, Adv. Mater. 13 (2001) 163–174.

[13] B. Walker, C. Kim, T.Q. Nguyen, Small molecule solution-processed bulk heterojunction solar cells, Chem. Mater. 23 (2011) 470–482.

[14] Y.W. Li, Q. Guo, Z.F. Li, J.N. Pei, W.J. Tian, Solution processable D-A small molecules for bulk-heterojunction solar cells, Energy Environ. Sci. 3 (2010) 1427–1436.

[15] M. Lloyd, J. Anthony, G. Malliaras, Photovoltaics from soluble small molecules, Mater. Today 10 (2007) 34–41.

[16] J. Roncali, Molecular bulk heterojunctions: an emerging approach to organic solar cells, Acc. Chem. Res. 42 (2009) 1719–1730.

[17] S. Loser, C.J. Bruns, H. Miyauchi, R.P. Ortíz, A. Facchetti, S.I. Stupp, A naphthodithiophene-diketopyrrolopyrrole donor molecule for efficient solution-processed solar cells, J. Am. Chem. Soc. 133 (2011) 8142–8145.

[18] B. Walker, A.B. Tamayo, X.D. Dang, P. Zalar, J.H. Seo, A. Garcia, Nanoscale phase separation and high photovoltaic efficiency in solution-processed, small-molecule bulk heterojunction solar cells, Adv. Funct. Mater. 19 (2009) 3063–3069.

[19] H.X. Shang, H.J. Fan, Y. Liu, W.P. Hu, Y.F. Li, X.W. Zhan, A solution-processable starshaped molecule for high-performance organic solar cells, Adv. Mater. 23 (2011) 1554–1557.

[20] B. Yin, L.Y. Yang, Y.S. Liu, Y.S. Chen, Q.J. Qi, F.L. Zhang FL, Solution-processed bulk heterojunction organic solar cells based on an oligothiophene derivative, Appl. Phys. Lett. 97 (2010), 023303.

[21] Y.J. Cheng, S.H. Yang, C.S. Hsu, Synthesis of conjugated polymers for organic solar cell applications, Chem. Rev. 109 (2009) 5868–5923.

[22] R.K. Kanaparthi, J. Kandhadi, L. Giribabu, Metal-free organic dyes for dye sensitized solar cells: recent advances, Tetrahedron 68 (2012) 8383–8393.

[23] C. Wang, H. Dong, W. Hu, Y. Liu, D. Zhu, Semiconducting π-conjugated systems in field-effect transistors: a material odyssey of organic electronics, Chem. Rev. 112 (2012) 2208–2267.

[24] C. Di, F. Zhang, D. Zhu, Multi-functional integration of organic field-effect transistors (OFETs): advances and perspectives, Adv. Mater. 25 (2013) 313–330.

[25] J. Zaumseil, H. Sirringhaus, Electron and ambipolar transport in organic field-effect transistors, Chem. Rev. 107 (2007) 1296–1323.

[26] H. Yan, Z.H. Chen, Y. Zheng, C. Newman, J.R. Quinn, F. Dotz, M. Kastler, M. A. Facchetti, A high-mobility electron-transporting polymer for printed transistors, Nature 457 (2009) 679.

[27] H. Klauk, U. Zschieschang, J. Pflaum, M. Halik, Ultralow-power organic complementary circuits, Nature 445 (2007) 745.

[28] F.S. Kim, X.G. Guo, M.D. Watson, S.A. Jenekhe, High-mobility ambipolar transistors and High−gain inverters from a donor–acceptor copolymer semiconductor, Adv. Mater. 22 (2010) 478–482.

[29] M. Muccini, A bright future for organic field-effect transistors, Nat. Mater. 5 (2006) 605.

[30] R. Capelli, S. Toffanin, G. Generali, H. Usta, A. Facchetti, M. Muccini, Organic light-emitting transistors with an efficiency that outperforms the equivalent light-emitting diodes, Nat. Mater. 9 (2010) 496.

[31] M. Muccini, W. Koopman, S. Toffanin, The photonic perspective of organic light-emitting transistors, Laser Photonics Rev. 6 (2012) 258–275.

[32] (a) J. Roncali, Synthetic principles for bandgap control in linear π-conjugated systems, J. Chem. Rev. 97 (1997) 173–206;
(b) S. Zrig, P. Remy, B. Andrioletti, E. Rose, I. Asselberghs, K.J. Clays, Engineering tuneable light-harvesting systems with oligothiophene donors and mono- or bis-bodipy acceptors, Org. Chem. 73 (2008) 1563–1566.

[33] J. Yu, Y. Shirota, A new class of high-performance red-fluorescent dyes for organic electroluminescent devices, [7-Diethylamino-3-(2-thienyl)chromen-2-ylidene]-2,2-dicyanovinylamine and {10-(2-Thienyl)-2,3,6,7-tetrahydro-1H,5H-chromeno [8,7,6-ij]quinolizin-11-ylidene}-2,2-dicyanovinylamine, Chem. Lett. 31 (2002) 984–985.

[34] S.C. Lin, S.S. Sun, Amorphous 2, 3-substituted thiophenes: potential electroluminescent materials, Chem. Mater. 14 (2002) 1884–1890.

[35] (a) S. Destri, M. Pasini, C. Botta, W. Porzio, F. Bertini, L.J. Marchio, Synthesis and crystal structure and optical properties of fluorenic-core oligomers, Mater. Chem. 12 (2002) 924–933;
(b) M. Béra-Abérem, H.A. Ho, M. Leclerc, Functional polythiophenes as optical chemo-and biosensors, Tetrahedron 60 (2004) 11169–11173.

[36] G. Barbarella, M. Melucci, G. Sotgiu, The versatile thiophene: an overview of recent research on thiophene-based materials, Adv. Mater. 17 (2005) 1581–1593.

[37] D.J. Crouch, P.J. Skabara, M. Heeney, I. McCulloch, S.J. Coles, M.B. Hursthouse, Hexyl-substituted oligothiophenes with a central tetrafluorophenylene unit: crystal engineering of planar structures for p-type organic semiconductors, Chem. Commun. 11 (2005) 1465–1467.

[38] A. Facchetti, M.-H. Yoon, C.L. Stern, H.E. Katz, T.J. Marks, Building blocks for n-type organic electronics: regiochemically modulated inversion of majority carrier sign in perfluoroarene-modified polythiophene semiconductors, Angew. Chem. Int. Ed. 42 (2003) 3900–3903.

[39] G. Zhou, G. Qian, L. Ma, Y. Cheng, Z. Xie, L. Wang, X. Jing, F. Wang, Polyfluorenes with phosphonate groups in the side chains as chemosensors and electroluminescent materials, Macromolecules 38 (2005) 5416–5424.

[40] P. Wagner, A.M. Ballantyne, K.W. Jolley, D.L. Officer, Synthesis and characterization of novel styryl-substituted oligothienylenevinylenes, Tetrahedron 62 (2006) 2190–2199.

[41] J.P. Wuskell, D. Boudreau, M. Wei, L. Jin, R. Engl, R. Chebolu, A. Bullen, K. D. Hoffacker, J. Kerimo, L.B. Cohenb, M.R. Zochowski, L.M. Loewa, Synthesis, spectra, delivery and potentiometric responses of new styryl dyes with extended spectral ranges, J. Neurosci. Methods 151 (2006) 200–215.

[42] G. Ginocchietti, U. Mazzucato, A. Spalletti, Excited state behaviour of some thio-analogues of 1,3-distyrylbenzene, J. Photochem. Photobiol. A Chem. 196 (2008) 233–238.

[43] X. Yang, X. Jiang, Ch Zhao, R. Chen, P. Qina, L. Sun, Donor–acceptor molecules containing thiophene chromophore: synthesis, spectroscopic study and electrogenerated chemiluminescence, Tetrahedron Lett. 47 (2006) 4961–4964.

[44] Y.-S. Kim, S. Young-A, Synthesis of 2, 2-bithiophene based dye sensor and optical properties toward metal cations, Mol. Cryst. Liq. Cryst. 551 (2011) 163–171 (R.M. F).

[45] O.P. Klochko, I.A. Fedyunyayeva, S.U. Khabuseva, O.M. Semenova, E. A. Terpetschnig, L.D. Patsenker, Benzodipyrrolenine-based biscyanine dyes: synthesis, molecular structure and spectroscopic characterization, Dyes Pigments 85 (2010) 7–15.

[46] G. Grandolini, A. Martani, A. Fravolini, Benzobisthiazoles. VII. Synthesis and structure of benzobisthiazole isomers, Ann. Chim. 58 (1968) 1248–1267.

[47] S.P.G. Costa Batista, M. Belsley, C. Lodeiro, M.M.M. Raposo, Synthesis and characterization of novel (oligo)thienyl-imidazo-phenanthrolines as versatile p-conjugated systems for several optical applications, Tetrahedron 64 (2008) 9230–9238.

[48] E. Fischer, Calculation of photostationary states in systems A-B when only A is known, J. Phys. Chem. 71 (1967) 3704–3710.

[49] O.J. Sandberg, M. Nyman, S. Dahlstrom, S. Sanden, B. Torngren, J.-H. Smatt, R. Osterbacka, On the validity of MIS-CELIV for mobility determination in organic thin-film devices, Appl. Phys. Lett. 110 (2017) 153504.

[50] A.L. Dubas, A.R. Tameev, A.I. Zvyagina, A.A. Ezhov, V.K. Ivanov, B. König, V. V. Arslanov, O.L. Gribkova, M.A. Kalinina, Ultrathin polydiacetylene-based synergetic composites with plasmon-enhanced photoelectric properties, ACS Appl. Mater. Interfaces 9 (2017) 43838–43845.

[51] B. Zhang, C. Qin, J. Ding, L. Chen, Z. Xie, Y. Cheng, L. Wang, High-Performance all-polymer white-light-emitting diodes using polyfluorene containing phosphonate groups as an efficient electron-injection layer, Adv. Funct. Mater. 20 (2010) 2951–2957.

[52] S.D. Tokarev, Yu A. Sotnikova, A.V. Anisimov, Yu V. Fedorov, G. Jonusauskas, D. A. Lypenko, V.V. Malov, A.R. Tameev, E.I. Maltsev, O.A. Fedorova, Donor–acceptor (E)-2-[2-(2,2′-bithiophen-5-yl)vinyl]benzo[d]thiazole: synthesis, optical, electrochemical studies and charge transport characteristics, Mendeleev Commun. 29 (2019) 567–569.

[53] Y. Gao, A. Pivrikas, B. Xu, Y. Liu, W. Xu, P.H.M. van Loosdrecht, W. Tian, Measuring electron and hole mobilities in organic systems: charge selective CELIV, Synth. Met. 203 (2015) 187–191.

[54] R.A. Irgashev, N.A. Kazin, N.I. Makarova, I.V. Dorogan, V.V. Malov, A.R. Tameev, G.L. Rusinov, A.V. Metelitsa, V.I. Minkin, V.N. Charushin, Synthesis and properties of new π-conjugated imidazole/carbazole structures, Dyes Pigments 141 (2017) 512–520.

[55] J. Fang, B.H. Wallikewitz, F. Gao, G. Tu, C. Muller, G. Pace, R.H. Friend, W.T. S. Huck, Conjugated zwitterionic polyelectrolyte as the charge injection layer for high-performance polymer light-emitting diodes, J. Am. Chem. Soc. 133 (2011) 683–685.

[56] D.G. Georgiadou, M. Vasilopoulou, L.C. Palilis, I.D. Petsalakis, G. Theodorakopoulos, V. Constantoudis, S. Kennou, A. Karantonis, D. Dimotikali, P. Argitis, Conjugated zwitterionic polyelectrolyte as the charge injection layer for high-performance polymer light-emitting diodes, ACS Appl. Mater. Interfaces 5 (2013) 12346–12354.

[57] C.H. Yang, C.J. Bhongale, C.H. Chou, S.H. Yang, C.N. Lo, T.M. Chen, C.S. Hsu, Synthesis and light emitting properties of sulfide-containing polyfluorenes and their nanocomposites with CdSe nanocrystals: a simple process to suppress keto-defect, Polymer 48 (2007) 116–128 (Electron Supporting Information).